Stimulating electron competition with extreme-ultraviolet-initiated high-order harmonic generation

Kathryn R. Hamilton [1,*] Lynda Hutcheson [2,†] Hugo W. van der Hart [2] and Andrew C. Brown [2]
[1]*Department of Physics, University of Colorado Denver, Denver, Colorado 80204, USA*
[2]*Centre for Light Matter Interaction, School of Mathematics and Physics, Queen's University Belfast, Belfast BT7 1NN, United Kingdom*

(Received 6 October 2023; accepted 15 November 2023; published 12 December 2023)

We address extreme-ultraviolet (XUV) initiated high-order harmonic generation (XIHHG) in argon atoms observing a resonant enhancement of the high-energy harmonics when the XUV pulse energy is tuned to the well-known window resonance. We attribute this effect to a three-stage mechanism: excitation of the $3s3p^6\,4p$ window resonance, followed by field-assisted autoionization and strong-field driven recollision. We also verify that the observed effect is robust against intensity-averaging, increasing the possibility that it may be observed experimentally. The resonant XIHHG mechanism represents an important addition to the attosecond toolset, as experimental schemes to identify signatures of correlation have heretofore proved elusive.

DOI: 10.1103/PhysRevA.108.063105

I. INTRODUCTION

High-order harmonic generation (HHG) is arguably *the* central process of attosecond (as) physics. While many applications focus on the generation of attosecond laser pulses [1], the technique is also invaluable as a spectroscopic tool as it affords a sensitive probe of electronic and even nuclear dynamics on the sub-Angstrom (spatial) and subfemtosecond (time) scales [2,3]. In this paper, we investigate how atomic structure may affect HHG, when HHG is initiated by the resonant absorption of an XUV photon.

Usually, HHG is understood in terms of the semi-classical "three-step" or "simple-man's" model wherein an electron is (1) tunnel-ionized and (2) accelerated by a strong electric field before (3) recolliding with its parent ion, releasing its absorbed energy in the form of a high-energy photon [4]. The recollision encodes structural and dynamical information in the emitted light, and thus by a careful analysis of the harmonic spectrum, HHG is realized as a sensitive measurement tool [5,6].

Despite the success of high-order harmonic spectroscopy, the technique is severely limited by the initial step: tunnel ionization is inefficient and restricted to the outermost valence electrons. Indeed, the long-awaited goal of as-pump as-probe laser schemes can likely not be realized with existing HHG sources, as the intensity of the pulses produced is so limited by the conversion efficiency [7].

One way to circumvent these limitations is with the use of both an extreme ultraviolet (XUV) and infrared (IR) pulse such that HHG is initiated by XUV-induced photoionization rather than IR-induced tunnel ionization. This can both increase the HHG efficiency and, more relevantly for the present work, stimulate HHG with more deeply bound electrons. The potential efficiency gains of XUV-initiated HHG (XIHHG) were demonstrated theoretically in 2005 [8–10], and recently absorption of XUV photons during the tunneling ionization process has been shown to increase harmonic amplitudes in small molecules [11]. However, the complexity of modeling multielectron systems in strong fields has hindered progress on the treatment of nonvalence electrons in XIHHG. Several HHG schemes which employ an XUV pulse to modify a tunnel-ionized system have been examined theoretically [12,13], and XIHHG with core electrons has been studied in small molecules [14], and with inner-valence electrons in atoms [15] and ions [16].

Other applications of XIHHG include isolating and controlling long trajectories [17] and observing interference between photon- and tunneling-initiated recombination pathways [18]. Inverted schemes where XUV photons are absorbed during the recombination rather than ionization step have resulted in the generation of additional plateaus beyond the IR-driven harmonic cutoff [19–21], with applications to attosecond pulse metrology [22].

In a previous paper [15] we described the use of XIHHG to resolve the contribution of inner- and outer-valence electrons to the harmonic spectrum in neon, and noted that a key goal of this technique should be to identify signatures of correlation between electrons. The observation of such behavior is by no means trivial, as recent studies have shown, for instance, that any potentially interesting XUV-initiated processes are rendered invisible by strong-field ionization in XUV pump–IR probe photoelectron spectroscopy [23]. In this article we outline an XIHHG scheme that not only enables us to *observe* signatures of multielectron effects, but also to *control* them. Previously, we showed how autoionizing resonances affect low-order harmonic generation in argon [24]. Here, we investigate how these "window" resonances affect XIHHG,

*kathryn.r.hamilton@ucdenver.edu
†lhutcheson02@qub.ac.uk

and find that at moderate IR intensities autoionization from the XUV-pumped $3s3p^6\,4p$ state enhances the HHG yield around the cutoff region of the spectrum. The observation of harmonics arising from Rydberg states has also been reported for one-color (i.e., standard) HHG setups [25]. There, the population of the excited states was driven by the ramp-on of the IR, and the effect was to produce additional harmonics via the "e-HHG" (excited state HHG) mechanism. However, in the XIHHG scheme used in this study the use of the XUV pump pulse affords an additional control parameter to stimulate the process, and thereby assesses the role of the electron correlation.

This scheme requires accurate description of both the argon atomic structure including electron correlation and electron dynamics mediated by an IR laser. While these challenges have been surmounted separately in the fields of high-precision atomic physics and semi-classical modeling of strong-field processes, only a handful of methods exist which can handle them simultaneously. Among them, the *R* matrix with time-dependence (RMT) technique has been demonstrated in studies of strong-field processes including attosecond-transient absorption spectroscopy [26,27], electron rescattering from negative ions [28], electron dynamics in attosecond angular streaking [29,30], IR-mediated HHG [31,32], and XIHHG [15,16].

II. *R* MATRIX WITH TIME-DEPENDENCE METHOD

RMT is an *ab initio* technique which solves the time-dependent Schrödinger equation by employing the *R*-matrix paradigm, dividing configuration space into two separate regions [33]. In the inner region the time-dependent multielectron wave function is represented by an *R*-matrix basis with time-dependent coefficients. In the outer region, the wave function is expressed in terms of residual-ion states coupled with the radial wave function of the ejected electron and is expressed explicitly on a finite-difference grid. The two-region wave functions are then matched directly at the boundary in both directions. The method has recently been extended to include the description of arbitrary light fields [34], semi-relativistic effects including spin-orbit interaction [35], and molecular targets [36]. A complete description of the code can be found in Ref. [37].

The harmonic spectra are obtained by Fourier-transforming and squaring the time-dependent expectation value of either the dipole length or the dipole velocity [38]. Indeed, the spectra produced from both methods show excellent agreement with each other until well past the cutoff energy, which is used as a check for accuracy in our calculations. Spectra determined from the dipole length are presented in this paper.

III. CALCULATION PARAMETERS

The primary laser is a six-cycle, 1.8-μm pulse with an intensity of 5×10^{13} Wcm^{-2} and a three-cycle, sine-squared ramp on and off profile. This isolates the generation of the high-energy cutoff harmonics to a single trajectory on a single IR cycle [32], allowing greater resolution in determining the mechanism responsible for the increase in harmonic yield. In a recent experiment a similar IR pulse was used to produce 43 attosecond (as) soft-x-ray pulses [39]. Longer duration IR pulses elicit the same resonant increase in yield of the cutoff harmonics, however, the underlying mechanism is more difficult to interpret from these spectra due to multicycle interference effects between the cutoff trajectories and increased tunnel ionization. The XUV intensity is 0.1% of the IR intensity and is 15 fs in duration (except in Fig. 6), beginning with the IR pulse and ending at its penultimate peak. Unless otherwise stated, the XUV energy is 27 eV, chosen to pump the $3s3p^6\;4p$ state. These parameters are chosen to emulate the mechanism described in Ref. [15] wherein the XUV pulse populates Rydberg series converging onto an ionisation threshold, allowing tunnel-ionisation and subsequent HHG to be driven with the inner-valence electrons.

The argon target is described within an *R*-matrix inner region of radius 20 a_0 and an outer region of 2000 a_0. The finite-difference grid spacing in the outer region is 0.08 a_0 and the time step for the wave-function propagation is 0.24 as. The description of argon includes all available $3s^23p^5\,\epsilon\ell$ and $3s3p^6\,\epsilon\ell$ channels up to a maximum total angular momentum of $L_{\max}=107$. The continuum functions are constructed from a set of 50 *B*-splines of order 9 for each available angular momentum of the outgoing electron.

Importantly, we can also selectively include all doubly excited states of the type $3s^23p^4ndn'\ell$, which is key for the accurate description of the $3s3p^6\,np$ window resonances [40]. The $3s3p^6\;{}^2S$ state interacts strongly with the $3s^23p^4(^1D)nd$ series (see, for example, Ref. [41]). Hence, we could expect resonances of the type $3s3p^6np$ to interact strongly with resonances of the type $3s^23p^4ndn'\ell$ through the dielectronic interaction, and indirectly, through the laser field. Thus, by selective inclusion of the doubly excited states, the influence of the autoionising $(3s3p^6np)$ states can be controlled independently of the direct ionisation of the 3*s* electron.

IV. RESULTS

Figure 1 shows the harmonic spectrum produced by argon in the laser scheme outlined above for different expansion lengths in the atomic-structure description of Ar. The spectrum obtained from only the 1.8-μm pulse obtained using the full atomic-structure description is also shown for reference. The XIHHG spectrum shows a double plateau structure, at variance with the single plateau of the 1.8-μm spectrum. The cutoff energies marked by the cross and star correspond to classical cutoff energies calculated with the binding energy of the 3*s* and 3*p* electrons, respectively [15,43]. These are in good agreement with the principal cutoff of the 1.8-μm spectrum (generated by tunnel-ionized 3*p* electrons) and the second cutoff of the XIHHG spectrum (generated by tunnel-ionized 3*s* electrons). However, the principal cutoff of the XIHHG spectrum is significantly reduced from this classically predicted value, as the photoionized 3*p* electrons are born into the continuum with around 11-eV energy, which reduces the cutoff to approximately 58 eV (diamond). To confirm the source of the high-energy harmonics, we perform the calculation removing the $3s3p^6\;{}^2S$ ionization threshold from the atomic structure description. This eliminates the contribution of the 3*s* electron [15,24]. The corresponding spectrum in Fig. 1 (green dots) indeed shows that the second plateau is

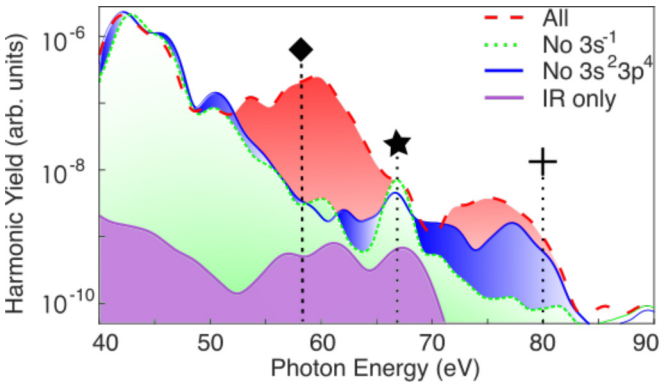

FIG. 1. The smoothed cutoff harmonics produced by argon in a mixed 1.8-μm and 27-eV laser pulse scheme. The figure shows the "full" spectrum (red dashes), the spectrum neglecting the action of the 3s electron (green dots), the spectrum not including the $3s^2 3p^4\, ndn'\ell$ Rydberg states (solid blue), and the spectrum produced by the IR pulse only (purple dot-dash). The double plateau structure is marked by the classically calculated cutoff energy for the 3p (star) and 3s (cross) electrons. Also shown is the cutoff energy calculated for photoionized 3p electrons (diamond).

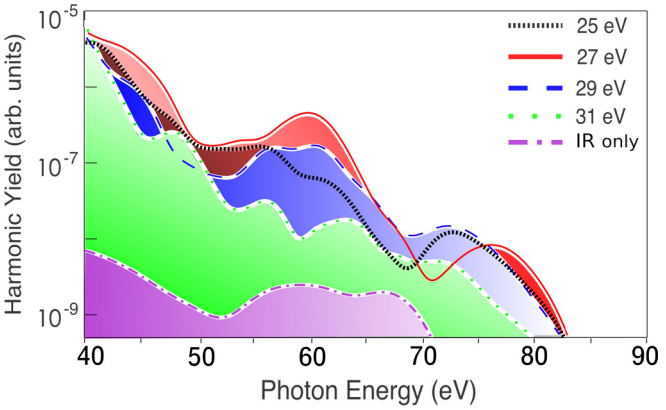

FIG. 3. Harmonic response of argon for a variety of XUV photon energies: 25 eV (vertical dashed black), 27 eV (solid red), 29 eV (horizontal dashed blue), and 31 eV (dotted green). The IR only spectrum is shown for reference (dot-dash purple). Detuning the XUV pulse energy from the window resonance (≈ 27 eV) suppresses the enhancement in yield.

removed in the absence of the 3s electron. This is in line with previous calculations for neon [15].

The most prominent feature in the spectrum is in the range between 55 and 65 eV where the calculation incorporating the full atomic structure yields harmonics enhanced by up to two orders of magnitude. To rule out any direct effect of the XUV pulse or atomic resonances we perform a time-frequency analysis on the spectrum (Fig. 2) by taking a Gabor transform [44,45] of the time-dependent dipole expectation values. The harmonics in the 55- to 65-eV energy range are produced around the zeros of the IR field, in line with the predictions of the three-step model [46], thus strongly indicating that this enhancement arises from strong-field-driven recollision dynamics of the electronic wave packet. Harmonic emission at 60 eV is dominant at the electric-field node prior to the peak

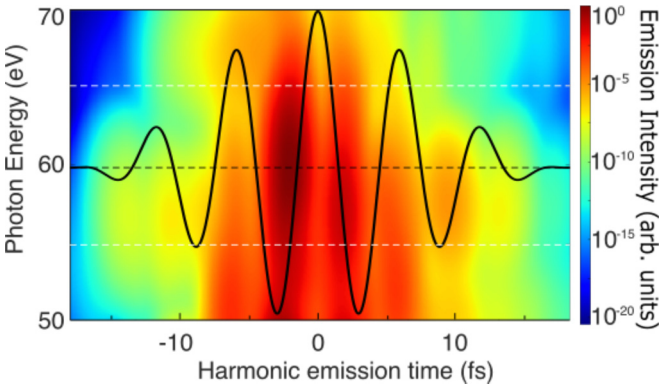

FIG. 2. Time-frequency decomposition of the harmonic emission from argon in a mixed 1.8-μm and 27-eV laser pulse scheme. The emission time is shown relative to the peak of the IR pulse, which is overlayed for reference. The strong emission in the 55- to 65-eV energy range coincides with a recollision event at −2.0 fs, indicating that the source of the emission is a strong-field-driven recollision process.

of the IR pulse, which is consistent with a harmonic response initiated by the emission of an energetic electron. This is consistent with supporting classical trajectory calculations, which suggest that cutoff energies around 60 eV are only obtained for trajectories launched before the peak of the IR pulse.

At energies below the 3p cutoff we do not expect to observe any influence of the 3s electron (as the ionization probability for the 3s is 3000 times lower than for the 3p with the present laser parameters), but only the calculation incorporating the full atomic structure displays the strong emission in this 55- to 65-eV range. Previous results for neon suggest that this emission is unlikely to be due to a direct contribution of the 3s, and thus we seek an alternative explanation. It is well known that, at photon energies around 27 eV, strong, resonant excitation of the 3s electron into the $3s3p^6\, np$ states actually suppresses photoionization of the 3p electron [40]. We showed in a previous study that these "window resonances" imprint on harmonic generation driven by higher-energy (390 nm) laser pulses [24]. We note that while the role of autoionizing states in traditional (one-color) HHG has been investigated previously both theoretically by Strelkov [47] and experimentally by Fareed *et al.* [48], these studies involved the recombination of a laser-driven electron into an autoionizing state, resulting in resonant harmonic generation, and thus differ from the present scheme where autoionization is the initial step in the mechanism. To our knowledge, the autoionization process itself (wherein a 3p electron decays into the 3s hole, promoting the excited electron into the $3p^{-1}$ continuum) has not yet been observed in HHG. Another significant difference between this work and other resonant harmonic generation schemes is that here the gain in harmonic yield is realized as a broad (≈ 10eV) enhancement of the cutoff harmonics, rather than a narrow (≈ 30 meV) increase in yield at the autoionizing state energy [48].

To probe the influence of autoionization in the present scheme, we remove all doubly excited configurations of the residual Ar^+ ion from the atomic structure description while retaining the $3s3p^6\ ^2S$ ionization threshold. This changes the

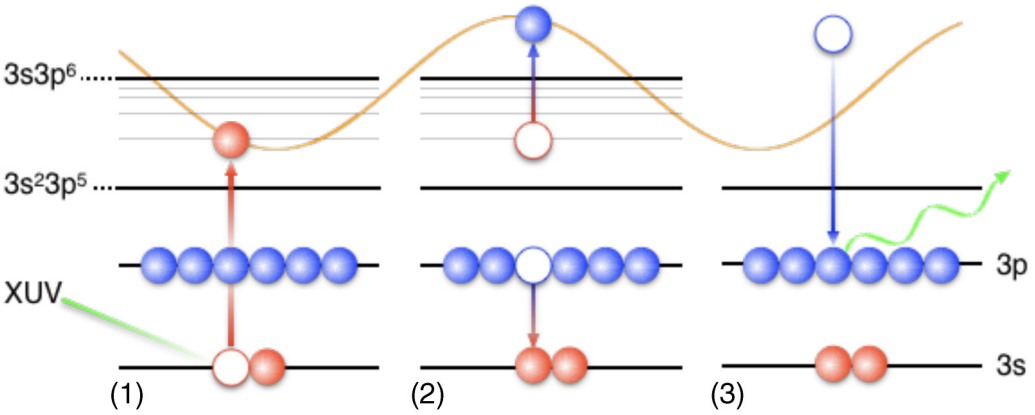

FIG. 4. Proposed three-stage mechanism for the source of resonant enhancement in XIHHG of argon: (1) A $3s$ electron is promoted by the XUV pulse into a $3s3p^6\ np$ state. (2) A $3p$ electron decays to the $3s$ hole promoting the excited electron into the $3p^{-1}$ continuum via (field-assisted) autoionization. (3) The ionized electron is driven to recollision by the strong field yielding HHG.

energy of the $3s3p^6\ 4p$ state and we adjust the XUV energy accordingly, but, importantly, it also drastically changes the shape of the $4p$ resonance [40]. Effectively, the reduced atomic structure description allows excitation and ionisation of both $3s$ and $3p$ electrons, but suppresses the autoionization pathway.

In the corresponding spectrum in Fig. 1 (solid blue), we *do* observe the second plateau due to photoionization of the $3s$ electron. However, the enhancement in yield in the 55- to 65-eV range is absent, confirming this feature is not caused by a direct contribution from the $3s$ electron.

Additionally, detuning the XUV pulse energy from the window resonance also suppresses the enhancement (shown in Fig. 3), as does reducing the XUV intensity (not shown). We propose, based on these behaviors, the following mechanism, depicted in Fig. 4, as the source of this enhancement. Stage 1: A $3s$ electron is promoted into the $3s3p^6\ 4p$ state by the XUV pulse. Stage 2: Autoionization: A $3p$ electron decays into the $3s$ hole releasing the excited electron into the $3p^{-1}$ continuum. Finally, stage 3: The continuum electron is driven by the IR field to recollide with the parent ion and produce high harmonic radiation. Autoionization is affected by the presence of the IR field [49], and so the second stage might more accurately be termed "field-assisted autoionization."

Importantly, both autoionization and direct photoionization of the $3p$ result in the electron being "born" into the continuum with nonzero energy (equal to the difference in energy between the XUV photon energy and the binding energy of the $3p$ electron), which affects the ensuing trajectory in the strong field. Classical trajectory calculations [15,32] show that the corresponding cutoff energy is reduced from 66 eV (for tunnel-ionized $3p$ electrons) to 58 eV (for autoionized or photoionized $3p$ electrons). This is borne out in the harmonic spectra (Fig. 1). Moreover, the cutoff is not reduced in calculations neglecting the autoionization pathway showing that direct photoionization of $3p$ electrons is not the source of the enhancement.

To probe this mechanism further we investigate the effect of the IR intensity. Figure 5 shows the enhancement for four different IR intensities, from 4–7 $\times$ 10^{13} Wcm^{-2}. The shift of the cutoff due to the excess energy of the autoionized electron is in line with classical trajectory calculations. The position of the resonance moves with the expected cutoff energy, and at higher intensity, the enhancement spans a broader energy range. This is in line with the expectation of our proposed mechanism: a stronger field elicits a broader range of return velocities for electrons ionized around the pulse peaks. At insufficiently high intensity, tunnel ionization is strongly suppressed. At high intensity we expect that the direct tunnel ionization of $3p$ electrons should dominate the harmonic spectrum, and including the autoionizing pathway, makes less of a difference. At intensities around 5×10^{13} Wcm^{-2} the resonant (autoionization) and nonresonant (tunnel-ionization) pathways are in balance and we observe the largest difference between the two spectra (around a 30 times enhancement for these pulse parameters).

Finally, we investigate the effect of the XUV pulse length on the yield. The yield enhancement is calculated by taking the ratio of the cumulative yields of the "full" and $3p$-only spectra between 55 and 65 eV. We find that independent of

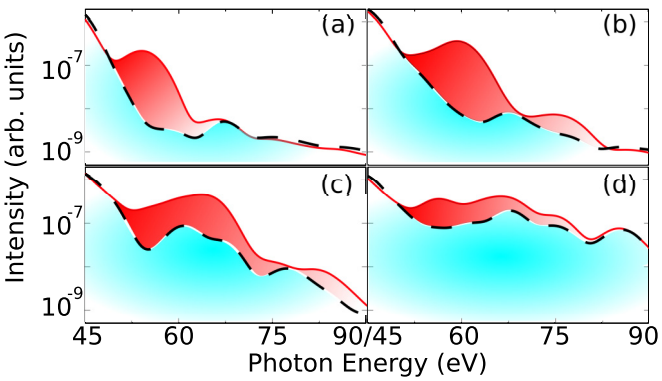

FIG. 5. Smoothed harmonics in the 45–90 eV range for four different IR intensities [(a) 4×10^{13}, (b) 5×10^{13}, (c) 6×10^{13}, and (d) 7×10^{13} Wcm^{-2}]. Both the "full" spectrum (solid red) and that neglecting the $3s$ electron (black dashes) are shown. The enhancement is the region bounded by the two spectra (dark, red shading).

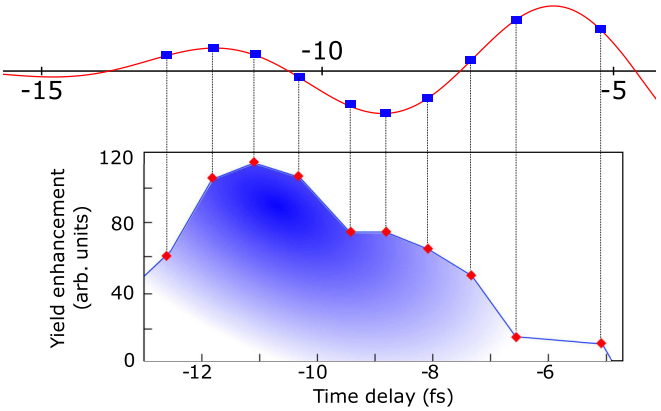

FIG. 6. Gain in cumulative harmonic yield in the 55–65 eV range for a variety of time delays (measured between the end of the XUV pulse and the peak of the IR pulse). The IR pulse is shown (top) for reference. The end of the XUV pulse for various time delays is marked with blue squares or red diamonds.

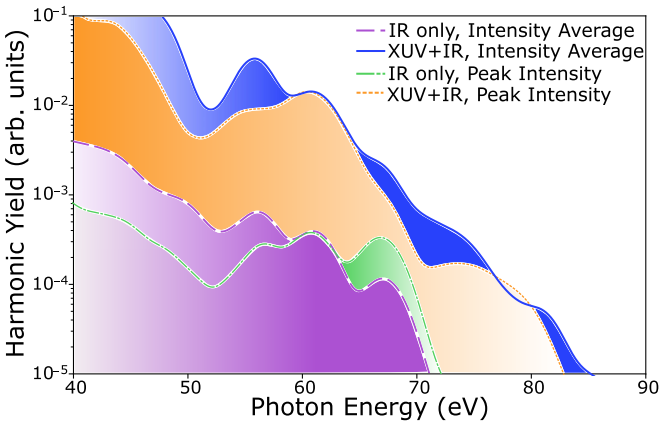

FIG. 7. Smoothed harmonic response of argon when irradiated by an IR only pulse and by a mixed two-color laser scheme. Shown are results at a single, peak intensity (5×10^{13} Wcm^{-2}) and results which have been focal-volume averaged.

time delay, at least 60 cycles (9 fs) of the XUV pulse are required to see any gain in yield. Figure 6 shows the yield enhancement as a function of XUV time delay for a 60-cycle XUV pulse. (The time delay is measured between the end of the XUV pulse and the peak of the IR). The largest enhancement in the yield is obtained when the XUV pulse has a delay of around −11 fs. Interestingly, when the XUV pulse remains "on" beyond this delay, the resonant yield is actually suppressed.

This lends weight to our proposed mechanism: if the XUV pulse is too short, we do not sufficiently populate the $3s3p^6\,4p$ state, as required for stage 1. If the time delay is too small, the $3s3p^6\,4p$ has insufficient population to start the three-step process to generate harmonic emission at the critical time of −2 fs: the wave packet generating the HHG signature must be created no later than a time of about −7 fs. Thus the XUV pulse must arrive sufficiently ahead of the NIR pulse to allow substantial (photoassisted) autoionization to occur. Given that (neglecting the influence of the IR) the autoionizing state decays in approximately 8 fs [49], the time delays offering optimal enhancement of HHG are thus in line with the proposed mechanism.

V. MACROSCOPIC EFFECTS

Macroscopic effects will play a key role in the manifestation of this effect experimentally, in particular the phase matching of the resonant harmonics. One contributor to the phase mismatch of the resonant harmonics is the different refractive indices induced in the medium by the XUV and IR pulses [50]. Comparing the different effective refractive indices, calculated from relevant values in the literature [51–53], we predict that an added delay of less than 4 fs, which according to Fig. 6 would still produce a resonant boost in yield, can be achieved provided the depth of the argon gas jet is less than 6 mm [54].

Another key macroscopic effect which must be considered experimentally is focal volume averaging. Figure 7 shows harmonic spectra which have been intensity-averaged over a range of IR intensities up to a peak intensity of 5×10^{13} Wcm^{-2} using the method outlined in Ref. [55]. The enhancement of the harmonic yield between 55 and 65 eV persists after accounting for focal volume averaging. We also performed further calculations (not shown) using an attosecond pulse train rather than a long XUV pulse as the secondary pulse. Generating such a pulse train, and controlling its time delay with respect to the driving IR, is now standard practice in attosecond laboratories. With this laser regime we see a similar boost in the harmonic yield between 55 and 65 eV. Thus we are confident that probing this mechanism should be achievable experimentally.

VI. CONCLUSION

XIHHG presents an attractive means of studying electron interactions in atomic and molecular systems. Where previous studies focused on either the extension of the harmonic spectrum, or the efficiency gains offered by XIHHG, we here demonstrated the technique's promise for investigating the role of electron correlation in ultrafast dynamics. By selecting the XUV energy to populate the $3s3p^6\,4p$ Rydberg state in Ar, we observed an enhancement in the HHG yield which could not be accounted for by the direct contribution of either the $3s$ or $3p$ electrons. Instead, we found that the enhancement appears in the spectra only when *both* the $3s$ and $3p$ ionization channels are open, *and* all doubly excited configurations of the residual Ar^+ ion were included in the calculation. Based on previous investigations which used the same R-matrix basis we can then associate this resonant enhancement with an autoionization pathway taking $3s3p^6\,4p$ to $3s^23p^5\,\epsilon\ell$.

We thus proposed a "three-stage" mechanism, where 1() the XUV excitation of the inner valence electron is followed by (2) field-assisted autoionization before (3) the ionized electron is driven on a recollision trajectory by the IR field. This resonant enhancement of ionization leads to a corresponding enhancement in the HHG yield and a reduction in the cutoff energy, associated with the classical trajectory described by an electron "born" into the IR field with nonzero velocity.

Increasing the IR intensity causes the resonant feature to span a broader energy range below the increased cutoff energy, and the amplitude of the resonant effect is reduced as the direct tunnel ionization of $3p$ electrons begins to dominate the spectrum. We also find that the XUV pulse must be at least 60 cycles in duration (to ensure sufficient population of the $3s3p^6\ 4p$ state) and must be timed to allow the autoionizing state to decay at a subsequent peak of the IR field. After performing intensity volume averaging on our results, we still obtain an enhancement of the harmonic yield associated with the proposed mechanism, suggesting that the mechanism should be experimentally observable.

While these results lend weight to the proposed mechanism, the time-dependent evolution of the state is not elucidated by this study, as the observable is tied to the strong-field continuum dynamics rather than the underlying atomic physics. However, a study which probed only the bound state dynamics (for example, by employing techniques of attosecond transient absorption spectroscopy) could shed further light on the process, and will be the basis of subsequent research into this system.

The interest in the present study, however, is the interaction between the atomic physics at play in the correlation induced dynamics (autoionization), and the "simple-man" physics driven by the strong field. To increase the contrast between the two regimes we chose, in this and previous studies [15], to employ a 1.8-μm IR pulse. This effectively reduces the direct HHG yield, while supporting sufficiently high-energy harmonics wherein we can observe the action of the inner-valence electrons. It is hard to speculate if this mechanism should persist for other target atoms, or indeed, in the commonly used 800-nm laser regime, as it depends heavily on the relative importance of the autoionization and tunnel-ionization pathways. However as 1.8 μm lasers become increasingly more available (see, e.g., Ref. [39]), it is our hope that combined XUV + 1.8 μm laser pulse schemes will provide the possibility for stimulating and observing resonant processes, particularly those which impact the cutoff harmonics.

The data used in this paper may be found using Ref. [42]. The RMT code is part of the UK-AMOR suite and can be obtained for free at Ref. [56].

ACKNOWLEDGMENTS

This work benefited from computational support by CoSeC, the Computational Science Centre for Research Communities, through CCPQ. K.R.H. was supported by the United States National Science Foundation under Grants No. OAC-1834740 and No. PHY-1803844, and the Department for Employment and Learning Northern Ireland under the program for government. A.C.B. and H.W.v.d.H. acknowledge funding from the EPSRC under Grants No. EP/T019530/1, No. EP/P022146/1, No. EP/P013953/1, No. EP/R029342/1 and No. EP/V05208X/1. This work relied on the ARCHER UK National Supercomputing Service, for which access was obtained via the UK-AMOR consortium funded by EPSRC. The authors would also like to thank C. P. Ballance for performing additional supporting calculations, and G. F. Gribakin for comments on the manuscript.

[1] M. Chini, K. Zhao, and Z. Chang, The generation, characterization and applications of broadband isolated attosecond pulses, Nat. Photon. **8**, 178 (2014).

[2] O. Smirnova, Y. Mairesse, S. Patchkovskii, N. Dudovich, D. Villeneuve, P. B. Corkum, and M. Y. Ivanov, High harmonic interferometry of multi-electron dynamics in molecules, Nature (London) **460**, 972 (2009).

[3] J. Itatani, J. Levesque, D. Zeidler, H. Niikura, H. Pépin, J. C. Kieffer, P. B. Corkum, and D. M. Villeneuve, Tomographic imaging of molecular orbitals, Nature (London) **432**, 867 (2004).

[4] P. B. Corkum, Plasma perspective on strong field multiphoton ionization, Phys. Rev. Lett. **71**, 1994 (1993).

[5] O. Smirnova and O. Gessner, Attosecond spectroscopy, Chem. Phys. **414**, 1 (2013).

[6] P. B. Corkum, Recollision physics, Phys. Today **64**, 36 (2011).

[7] P. B. Corkum and F. Krausz, Attosecond science, Nat. Phys. **3**, 381 (2007).

[8] M. B. Gaarde, K. J. Schafer, A. Heinrich, J. Biegert, and U. Keller, Large enhancement of macroscopic yield in attosecond pulse–train assisted harmonic generation, Phys. Rev. A **72**, 013411 (2005).

[9] J. Biegert, A. Heinrich, C. P. Hauri, W. Kornelis, P. Schlup, M. P. Anscombe, M. B. Gaarde, K. J. Schafer, and U. Keller, Control of high-order harmonic emission using attosecond pulse trains, J. Mod. Opt. **53**, 87 (2006).

[10] G. Gademann, F. Kelkensberg, W. K. Siu, P. Johnsson, M. B. Gaarde, K. J. Schafer, and M. J. J. Vrakking, Attosecond control of electron-ion recollision in high harmonic generation, New J. Phys. **13**, 033002 (2011).

[11] J. Wang, A. Liu, and K.-J. Yuan, High-order harmonic generation in aligned molecules by combination of weak XUV and intense IR laser pulses, Opt. Commun. **460**, 125216 (2020).

[12] C. Buth, M. C. Kohler, J. Ullrich, and C. H. Keitel, High-order harmonic generation enhanced by XUV light, Opt. Lett. **36**, 3530 (2011).

[13] M. Tudorovskaya and M. Lein, High-harmonic generation with combined infrared and extreme ultraviolet fields, J. Mod. Opt. **61**, 845 (2014).

[14] J. Leeuwenburgh, B. Cooper, V. Averbukh, J. P. Marangos, and M. Ivanov, High-order harmonic generation spectroscopy of correlation-driven electron hole dynamics, Phys. Rev. Lett. **111**, 123002 (2013).

[15] A. C. Brown and H. W. van der Hart, Extreme-ultraviolet-initated high-order harmonic generation: Driving inner-valence electrons using below-threshold-energy extreme-ultraviolet light, Phys. Rev. Lett. **117**, 093201 (2016).

[16] D. D. A. Clarke, H. W. van der Hart, and A. C. Brown, Extreme-ultraviolet-initiated high-order harmonic generation in Ar^+, Phys. Rev. A **97**, 023413 (2018).

[17] M. Krüger, D. Azoury, B. D. Bruner, and N. Dudovich, The role of electron trajectories in XUV-initiated high-harmonic generation, Appl. Sci. **9**, 378 (2019).

[18] W. Dong, H. Hu, and Z. Zhao, Time-resolved recombination by attosecond-controlled high harmonic generation, Opt. Express **28**, 22490 (2020).

[19] A. V. Flegel, M. V. Frolov, A. N. Zheltukhin, and N. V. Vvedenskii, Quasi-classical model of electron rescattering in fields of intense infrared and weak high-frequency laser pulses, Quantum Electron. **47**, 222 (2017).

[20] T. S. Sarantseva, M. V. Frolov, and N. V. Vvedenskii, Modification of the spectrum of high harmonics by a weak vacuum ultraviolet field, Quantum Electron. **48**, 625 (2018).

[21] T. S. Sarantseva, M. V. Frolov, N. L. Manakov, A. A. Silaev, N. V. Vvedenskii, and A. F. Starace, XUV-assisted high-order-harmonic-generation spectroscopy, Phys. Rev. A **98**, 063433 (2018).

[22] T. S. Sarantseva, M. V. Frolov, N. L. Manakov, A. A. Silaev, A. A. Romanov, N. V. Vvedenskii, and A. F. Starace, Attosecond-pulse metrology based on high-order harmonic generation, Phys. Rev. A **101**, 013402 (2020).

[23] C. Gao, P. M. Dinh, P. Reinhard, and E. Suraud, Towards the analysis of attosecond dynamics in complex systems, Phys. Chem. Chem. Phys. **19**, 19784 (2017).

[24] A. C. Brown, S. Hutchinson, M. A. Lysaght, and H. W. van der Hart, Interference between competing pathways in atomic harmonic generation, Phys. Rev. Lett. **108**, 063006 (2012).

[25] S. Beaulieu, S. Camp, D. Descamps, A. Comby, V. Wanie, S. Petit, F. Légaré, K. J. Schafer, M. B. Gaarde, F. Catoire, and Y. Mairesse, Role of excited states in high-order harmonic generation, Phys. Rev. Lett. **117**, 203001 (2016).

[26] M. Hartmann, L. Hutcheson, G. D. Borisova, P. Birk, S. Hu, A. Brown, H. Van der Hart, C. Ott, and T. Pfeifer, Core-resonance line-shape analysis of atoms undergoing strong-field ionization, J. Phys. B: At., Mol. Opt. Phys. **55**, 245601 (2022).

[27] T. Ding, C. Ott, A. Kaldun, A. Blättermann, K. Meyer, V. Stooss, M. Rebholz, P. Birk, M. Hartmann, A. Brown, H. V. D. Hart, and T. Pfeifer, Time-resolved four-wave-mixing spectroscopy for inner-valence transitions, Opt. Lett. **41**, 709 (2016).

[28] O. Hassouneh, S. Law, S. F. C. Shearer, A. C. Brown, and H. W. van der Hart, Electron rescattering in strong-field photodetachment of F^-, Phys. Rev. A **91**, 031404(R) (2015).

[29] G. S. J. Armstrong, D. D. A. Clarke, J. Benda, A. C. Brown, and H. W. van der Hart, Electron correlation and short-range dynamics in attosecond angular streaking, Phys. Rev. A **101**, 041401(R) (2020).

[30] W. Jiang, G. S. J. Armstrong, J. Tong, Y. Xu, Z. Zuo, J. Qiang, P. Lu, D. D. A. Clarke, J. Benda, A. Fleischer, H. Ni, K. Ueda, H. W. van der Hart, A. C. Brown, X. Gong, and J. Wu, Atomic partial wave meter by attosecond coincidence metrology, Nat. Commun. **13**, 5072 (2022).

[31] O. Hassouneh, A. C. Brown, and H. W. van der Hart, Harmonic generation by noble-gas atoms in the near-IR regime using *ab initio* time-dependent *R*-matrix theory, Phys. Rev. A **90**, 043418 (2014).

[32] K. R. Hamilton, H. W. van der Hart, and A. C. Brown, Pulse-shape control of two-color interference in high-order-harmonic generation, Phys. Rev. A **95**, 013408 (2017).

[33] L. R. Moore, M. A. Lysaght, L. A. A. Nikolopoulos, J. S. Parker, H. W. van der Hart, and K. T. Taylor, The RMT method for many-electron atomic systems in intense short-pulse laser light, J. Mod. Opt. **58**, 1132 (2011).

[34] D. D. A. Clarke, G. S. J. Armstrong, A. C. Brown, and H. W. van der Hart, *R*-matrix with time-dependence theory for ultrafast atomic processes in arbitrary light fields, Phys. Rev. A **98**, 053442 (2018).

[35] J. Wragg, D. D. A. Clarke, G. S. J. Armstrong, A. C. Brown, C. P. Ballance, and H. W. van der Hart, Resolving ultrafast spin-orbit dynamics in heavy many-electron atoms, Phys. Rev. Lett. **123**, 163001 (2019).

[36] J. Benda, J. D. Gorfinkiel, Z. Mašín, G. S. J. Armstrong, A. C. Brown, D. D. A. Clarke, H. W. van der Hart, and J. Wragg, Perturbative and nonperturbative photoionization of H_2 and H_2O using the molecular *R*-matrix-with-time method, Phys. Rev. A **102**, 052826 (2020).

[37] A. C. Brown, G. S. Armstrong, J. Benda, D. D. Clarke, J. Wragg, K. R. Hamilton, Z. Mašín, J. D. Gorfinkiel, and H. W. van der Hart, RMT: R-matrix with time-dependence. solving the semi-relativistic, time-dependent Schrödinger equation for general, multielectron atoms and molecules in intense, ultrashort, arbitrarily polarized laser pulses, Comput. Phys. Commun. **250**, 107062 (2020).

[38] A. C. Brown, D. J. Robinson, and H. W. van der Hart, Atomic harmonic generation in time-dependent *R*-matrix theory, Phys. Rev. A **86**, 053420 (2012).

[39] T. Gaumnitz, A. Jain, Y. Pertot, M. Huppert, I. Jordan, F. Ardana-Lamas, and H. J. Wörner, Streaking of 43-attosecond soft-x-ray pulses generated by a passively CEP-stable mid-infrared driver, Opt. Express **25**, 27506 (2017).

[40] P. G. Burke and K. T. Taylor, *R*-matrix theory of photoionization. Application to neon and argon, J. Phys. B: At. Mol. Phys. **8**, 2620 (1975).

[41] H. Smid and J. E. Hansen, The importance of continuum d states for the interaction $nsnp^6 \leftrightarrow ns^4d$ in the rare gases, J. Phys. B: At. Mol. Phys. **16**, 3339 (1983).

[42] A. C. Brown, XUV-initiated harmonic generation in argon, PURE research database (2023), doi:10.17034/525d17f6-3e79-4d15-a12a-2c64109eab7c.

[43] J. L. Krause, K. J. Schafer, and K. C. Kulander, High-order harmonic generation from atoms and ions in the high intensity regime, Phys. Rev. Lett. **68**, 3535 (1992).

[44] D. Gabor, Theory of communication, J. Inst. Electr. **93**, 429 (1946).

[45] C. C. Chirilă, I. Dreissigacker, E. V. van der Zwan, and M. Lein, Emission times in high-order harmonic generation, Phys. Rev. A **81**, 033412 (2010).

[46] M. Lewenstein, P. Balcou, M. Y. Ivanov, A. L'Huillier, and P. B. Corkum, Theory of high-harmonic generation by low-frequency laser fields, Phys. Rev. A **49**, 2117 (1994).

[47] V. Strelkov, Role of autoionizing state in resonant high-order harmonic generation and attosecond pulse production, Phys. Rev. Lett. **104**, 123901 (2010).

[48] M. A. Fareed, V. V. Strelkov, N. Thiré, S. Mondal, B. E. Schmidt, F. Légaré, and T. Ozaki, High-order harmonic generation from the dressed autoionizing states, Nat. Commun. **8**, 16061 (2017).

[49] H. Wang, M. Chini, S. Chen, C.-H. Zhang, F. He, Y. Cheng, Y. Wu, U. Thumm, and Z. Chang, Attosecond time-resolved autoionization of argon, Phys. Rev. Lett. **105**, 143002 (2010).

[50] N. Rosenthal and G. Marcus, Discriminating between the role of phase matching and that of the single-atom response in resonance plasma-plume high-order harmonic generation, Phys. Rev. Lett. **115**, 133901 (2015).

[51] P.-C. Li and S.-I. Chu, High-order-harmonic generation of ar atoms in intense ultrashort laser fields: An all-electron time-dependent density-functional approach including macroscopic propagation effects, Phys. Rev. A **88**, 053415 (2013).

[52] J. Zhang, Z. H. Lu, and L. J. Wang, Precision refractive index measurements of air, N_2, O_2, Ar, and CO_2 with a frequency comb, Appl. Opt. **47**, 3143 (2008).

[53] V. Loriot, E. Hertz, O. Faucher, and B. Lavorel, Measurement of high order Kerr refractive index of major air components, Opt. Express **17**, 13429 (2009).

[54] J. Rothhardt, S. Hädrich, S. Demmler, M. Krebs, S. Fritzsche, J. Limpert, and A. Tünnermann, Enhancing the macroscopic yield of narrow-band high-order harmonic generation by fano resonances, Phys. Rev. Lett. **112**, 233002 (2014).

[55] L. Hutcheson, H. W. van der Hart, and A. C. Brown, Modelling intensity volume averaging in *ab initio* calculations of high harmonic generation, J. Phys. B: At., Mol. Opt. Phys. **56**, 135402 (2023).

[56] A. C. Brown *et al.*, The RMT repository, https://gitlab.com/Uk-amor/RMT/rmt (2023).